Benajes, J.; Pastor, JV.; García Martínez, A.; Monsalve-Serrano, J. (2018). Redesign and characterization of a single-cylinder optical research engine to allow full optical access and fast cleaning during combustion studies. Experimental Techniques. 42(1):55-68. https://doi.org/10.1007/s40799-017-0219-9

Redesign and characterization of a single-cylinder optical research engine to allow full optical access and fast cleaning during combustion studies

Experimental Techniques, *Volume 42*, *February 2018*, *Pages 55-68*
https://doi.org/10.1007/s40799-017-0219-9

Jesús Benajes, José V. Pastor, Antonio García* and Javier Monsalve-Serrano

CMT-Motores Térmicos, Universitat Politècnica de València, Camino de Vera s/n, 46022 Valencia, Spain
* Corresponding author: angarma8@mot.upv.es; Tel.: +34-963-877-659

Abstract: This work describes the update of an optical engine design with the aim of increasing its capabilities when used for combustion studies. The criteria followed to perform the optical engine redesign were: maximize the optical accessibility to the combustion chamber, minimize the time consumed to clean the optical parts, and minimize the adaptation costs. To meet these requirements, a modular design using window-holders to fit the windows in the optical flange, was proposed. This novel solution allows optical access near the cylinder-head plane while maintaining high operating flexibility (i.e. fast transition between optical and metal engine, and very fast cleaning procedure).

The new engine design has three additional optical accesses to the combustion chamber and resulted in more efficient operation compared to the original design, reducing the time consumed to clean the optical parts from 40 down to 10 minutes. Two main parameters of the new engine were characterized, the effective compression ratio and the rotatory flow field velocity (swirl). The characterization process revealed very similar values between the effective and geometric compression ratios (14.7:1 vs 14.2:1), which confirms the use of appropriate dimensional tolerances during the machining process and low amount of blow-by. Finally, the swirl ratio was characterized through particle image velocimetry measurements for different crank timings at 1200 rpm and motored conditions, using the optical piston with a cylindrical bowl. This method revealed swirl ratios varying from 1 to 1.7 depending on the timing considered, with increasing trend as the piston moves towards the top dead center.

Keywords: Optical engine; Efficiency; Combustion; Swirl; Optimization

1. Introduction

Internal combustion engines (ICE) play a fundamental role in the lifestyle of modern societies [1]. The capability of ICEs to cover fundamental requirements such as people and goods transportation and power generation has resulted in their mass production [2]. However, the massive use of ICEs has contributed to the global energy consumption and pollutant emissions increase [3]. Since the engine-out emissions are harmful to both humans and the environment [4][5], stringent regulations have been introduced along the years to reduce progressively the negative impact of the ICEs [6]. This fact, combined with the improvement in the fuel economy demanded by the vehicle users, has brought new challenges to the engine research community and manufacturers.

The continuous optimization of the existing technologies and the development of new combustion systems needed to satisfy these demands, requires performing basic studies to allow the fundamental comprehension of the in-cylinder processes governing the pollutant emissions generation and performance of the ICEs [7][8].

The study of the different processes occurring inside the combustion chamber, e.g. the fuel injection process, air movement [9], fuel-air mixing and combustion, is typically addressed by using two complementary main sources of information: the experimental [10] and computational tools [11]. Figure 1 shows the different tools employed for experimentation, arranged from left to right by the degree of the fundamental understanding that they provide to the researchers. Also, the precision in controlling the boundary conditions

of the tests, decrease as moving to the right in the scheme, where the experimental facilities are closer to the production engine.

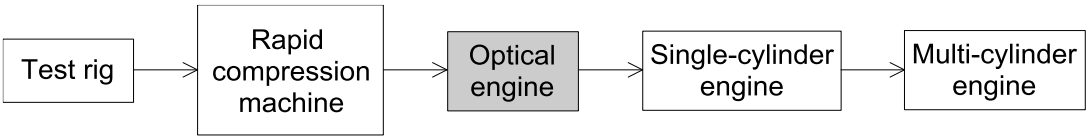

Figure 1. Different experimental research tools arranged from more fundamental (left) to more applied investigation (right).

The test rig is a constant volume vessel capable of reproducing the thermodynamic conditions existing in the combustion chamber of a real diesel engine when the injection starts, by means of a continuous flow of high temperature, high pressure gas through the test chamber [12]. This experimental device is endowed with different optical accesses, which allows the macroscopic study of the fuel injection event and combustion process by using different optical techniques [13]. Increasing the similarities to ICEs, the rapid compression machine (RCM) is typically used to study the autoignition chemistry by simulating a single engine compression stroke, which prevents the variations that appear during the real engine operation [14]. Optical techniques can be also applied in this device to determine the temperature and flow fields inside the reaction chamber and to measure the concentrations of several species produced during combustion [15]. Another fundamental research tool, closer to the real operation, is the optical engine [16]. This device is conceived to perform optical studies under the most similar conditions to the real engine operation. In this case, the experimental installation is based on a single-cylinder engine which has been modified to allow optical access to the combustion chamber, so that the flow fields inside the combustion chamber and also the cycle-to-cycle variations are more representative of the real engine behavior. By this reason, the optical engines are also typically used to validate, tune and refine the computational models used for modelling ICEs [17][18].

Single-cylinder engines (SCE) are devoted to carry out more applicate studies, such as performance [19] and engine-out emissions measurements [20], in highly controlled conditions. The test cell in which they are installed contain all the auxiliary systems for their operation and control, which are designed to minimize the variations in the intake conditions. This fact means that, ideally, the cycle-to-cycle variations during the engine operation are only consequence of variations in the combustion process itself. The observations using the optical engine can be used to understand the trends in engine-out emissions and performance measured here. Finally, the multi-cylinder engines (MCE) are the ones in production in the automotive industry [21]. They are installed in fully instrumented test cells capable of measuring performance and emissions. In this case, the auxiliary systems are those of the engine, so that the test cells result slightly simplified with respect to the SCE ones. The research done in this engine platform entails the most applicate work, e.g. to study the engine response to transient conditions, assess variations in engine hardware and perform homologation cycles [22].

Considering the challenge of achieving the emissions levels imposed by the future emissions regulations and the efficiency requirements imposed by vehicle users simultaneously, it is clear that more fundamental investigation is needed in the field of the ICEs. Literature demonstrates that the use of optical engines is essential for this task, since they allow to acquire fundamental understanding that otherwise would not be possible. Moreover, due to the great similarities to the real engines, the knowledge acquired can be directly extrapolated, contributing to the development of both compression ignition [23] and spark ignition engines [24]. In this sense, a wide variety of phenomena have been studied in detail, such as: the pilot injection process optimization through the liquid and vapor fuel visualization [25], the effect of swirl and tumble flows on the in-cylinder fuel-vapor distribution [26], the effect of biofuels on the air-fuel mixing and combustion behavior [27][28], the fuel injection characteristics governing the knocking phenomenon in spark ignition engines [29], the effect of coolant temperature on air-fuel mixture formation [30] and the distribution of the chemical species during the combustion process [31], among others.

In spite of the scientific advantages that they offer, operating with optical engines is more troublesome than with single-cylinder engines, and much more difficult than doing it with multi-cylinder engines. In this sense, the optical parts typically need to be cleaned in the middle of the tests campaign because of the soiling of the optical parts, which forces to stop the installation continuously. Also, depending on the optical engine design, great time is consumed between two consecutive tests to ensure the same thermodynamic conditions cycle-to-cycle. Finally, the application of advanced optical techniques to study some in-cylinder phenomena

requires the engine to have several optical accesses [32], which increases the complexity of the design and costs compared to the equivalent single-cylinder engines.

Different solutions can be found in literature regarding the optical engine designs [33][34][35]. The basic idea of all these designs is to use a Bowditch-style extended piston [36] to connect two pistons, as will be described in detail in the next section. The lower-piston is a regular piston that runs inside a conventional engine block, while the upper-piston has at least one optical access to allow performing optical studies, and it is called optical piston. Then, both pistons are connected using an empty cylindrical part, typically called extended or elongated piston. The major differences between the designs found in literature are related to the optical accessibility capacity to the cylinder. Thus, while some designs only have a single optical access through the piston bowl using a 45° mirror placed in the middle of the elongated piston [37], other designs have multiple accesses [38], which broadens the optical techniques that can be applied to study a given phenomenon [39]. In particular, the addition of multiple accesses offers the possibility of applying laser techniques, which typically require introducing laser sheets to the cylinder, parallel to the cylinder head plane. To allow this, different solutions are found in literature. The most optically accessible engines are those designed with full transparent liners [40][41]. These designs rely on using sapphire liners to allow optical access to the cylinder during almost the complete engine cycle. However, the cost of this solution is quite expensive, being restricted its acquisition to a small portion of engine research centers. To reduce the cost, alternative designs use pent roof windows inserted in the cylinder liner [42], and some other designs propose using a short quartz ring placed between the liner and cylinder head [43]. Both solutions are effective in conferring optical access to the combustion chamber at the cylinder head plane level, however, the cleaning of the inner side of these windows is not fast because some other elements should be removed to allow this task. In addition, the disposition of the windows can reduce drastically the compression ratio and/or increase the gas volume in the crevices.

Considering this background, the work presented in this paper describes the improvement of an existing optical engine design with the aim of increasing the capabilities of the installation to apply fundamental studies, as well as to increase the operational efficiency of the test cell. Thus, the main objective is to reach a modular design that allows minimizing the challenges found during the operation with optical engines, i.e. reduce the cleaning time and increase the optical accessibility. For this purpose, firstly, the original design is explained to state the motivation of the work. Later, the process followed to update the optical engine design is described. Lastly, to assess if the final characteristics of the redesigned engine are representative of those of the real engines, the engine compression ratio and swirl ratio are characterized by means of dedicated studies.

2. Description of the original single-cylinder optical engine

This section is devoted to describe the original single-cylinder optical engine, which allows to comprehend the main restrictions of the original design. The main characteristics of the engine are summarized in table 1. It is interesting to note that the engine can be also used for spark ignition experiments using an appropriate cylinder head. In this sense, the authors have tested the spark ignition concept using a modified compression ignition cylinder head, in which a hole was machined to include the spark plug [16].

Table 1. Main characteristics of the engine.

Parameter	Value
Type	CI, 4stroke, DI
Max. engine speed	1200 rpm
Bore	85 mm
Stroke	96 mm
Bowl diameter	45 mm
Bowl depth	12 mm

The operating principle of the optical engine can be understand looking at the figure 2, which shows a cross sectional view of the optical engine (left) and the optical layout necessary to study the injection and combustion processes (right). Different elements can be identified from the cross sectional view. In the top

part, it can be identified the center-mounted direct injector and the optical piston with a cylindrical sapphire window placed in the bottom part of the piston bowl. This optical piston is screwed on the piston-extensor, which connects the optical piston with the lower piston to make their movement solidary. The cylindrical piston-extensor is empty to allow accommodating an elliptical 45° mirror in the middle of the optical path, below the piston bowl sapphire window. With this set-up, in-cylinder images can be recorded with a fast camera through the elliptical mirror, as can be seen in the right-side subfigure. In the bottom part of the engine, it is possible to distinguish the regular piston, on which the piston-extensor is screwed, the cylinder-liner and the engine block. Finally, in the outer part of the system, there is a metal piece referred to as topwork that maintains the relative distance between the engine block and the cylinder-head, and also guides the optical piston. It is interesting to note that, since the optical piston is not lubricated with any fluid, Teflon rings are used. The use of this material allows to ensure the sealing between the optical piston and the inner part of the cylinder-liner to avoid the in-cylinder gas leakage (blow-by). However, the easy degradation of the Teflon under high temperature conditions limits the maximum engine speed and the effective operating hours of the installation.

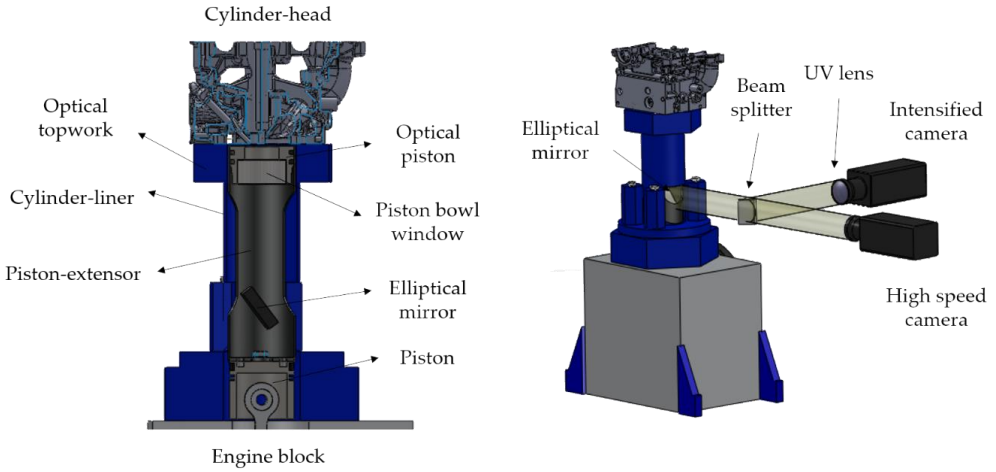

Figure 2. Cross sectional view of the optical engine (left) and optical layout necessary to study the combustion process (right).

Figure 3 shows an example of the images acquired with this type of engine design. The left-side subfigure shows the injection process of gasoline fuel at high injection pressure using a 7-hole injector nozzle. From the figure, it can be identified two intake valves (upper part), one exhaust valve, the center-mounted direct injector, a spark plug and a pressure sensor. This type of images allow to study fundamental parameters related to the injection and mixing process, such as the length of the liquid and vapor phase of the fuel, which are key parameters governing the pollutant emissions formation [44]. The second and third subfigure show images taken during the combustion development. In particular, the second subfigure shows the natural luminosity emitted during the combustion process, acquired with a high speed camera, while the third one is colored based on the OH* radical intensity, which was acquired using an intensified camera equipped with an ultraviolet lens and a 310 nm band pass filter [45]. This type of results serve to trace the high temperature zones in the combustion chamber, which is relevant to study, for example, the NOx emissions.

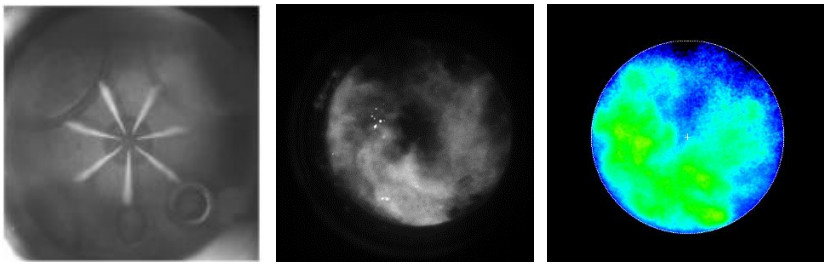

Figure 3. In-cylinder images of the injection (left) and combustion process (middle and right) acquired through the piston bowl window.

During the operation with the original engine configuration, several problems arise. As explained in the introduction section, the combustion products make the sapphire window of the piston to get dirty, which directly affects to the quality of the images taken and to the intensity levels captured with the high speed cameras, thus distorting the results of the study. To clean the inner side of the sapphire window, the disassembly of the optical piston is needed. This operation entails several actions: remove the elliptical mirror, place the optical piston in the bottom dead center (BDC) position by actuating manually on the crankshaft, introduce a dedicated tool to unscrew the piston window, clean the window, and reassembly all the parts. During the reassembly process, the elliptical mirror should be aligned again with the cameras to ensure recording the same in-cylinder area, and the cameras should be put in focus again, which implies an extra time consumed. The mean time consumed to perform all these tasks is about 40 min every 30 combustion cycles.

The major source of operating inefficiency of the original engine design, is the necessity of removing the cylinder-head to change the piston rings, or the piston itself. This kind of operations take around 4 or 5 hours due to the necessity of disassembly the cylinder-head completely. It is worthy to note that, since the material used for the piston rings is Teflon, and it degrades rapidly at high temperatures, this task has to be done several times in not too much operating hours. For example, when running the engine at a moderated speed of 1200 rpm, typically used because of the natural frequency of the pulsed lasers, the piston rings degrade after 10 minutes of operation. Thus, with the aim of avoiding this shortcomings, a new engine design has been performed and validated as described in next sections.

3. Engine design update and characterization

This section contains the main details of the engine design update process. The first subsection is dedicated to define the new optical engine design, which serves to highlight the benefits compared to the original version. The last subsection describes the engine characterization in terms of effective compression ratio and swirl ratio, and presents a validation of the new design under combustion conditions.

3.1. Description of the new design

The engine design update was conditioned by three main requirements:

- Maximize the optical accessibility and versatility for different studies
- Minimize the time consumed to clean the optical parts (maximize the operating efficiency of the engine test bench)
- Minimize the cost of the new version by using the original piston extensor

To fulfill these requirements, a modular design was proposed instead of using a single piece top work. In the new design, the outer metal part of the original design (top work) was substituted by different elements, as shown in figure 4. Firstly, four columns were used to maintain the relative distance between the engine block and the cylinder-head. Also, a mobile cylinder-liner with a water-cooled housing was used. This allowed to clean the piston window in a faster way (around 4 minutes), by only removing four screws and moving down the cylinder-liner and housing (figure 5).

To increase the optical accessibility to the combustion chamber, some additional optical accesses were done in the spatial plane near the cylinder-head. To do this, a new optical flange was designed, in which all the optical parts were assembled. To gain flexibility and operating efficiency, each window was embedded in a window-holder, which is later inserted and screwed in the optical flange. This system allows to extract and clean the windows in around 2 minutes each, when needed. The use of windows-holders also enables the substitution of the windows by metal dummies, which prevents damaging the optical parts if the optical access is not required in the tests campaign. If the soiling degree of the inner surfaces of the windows is not excessive, they can be cleaned without removing the windows-holders, accessing directly by hand through the gap between the optical flange and the cylinder-liner in the cleaning position (figure 5). It is worthy to note that the shape of the outer surface of these windows is planar, while the inner part is rounded to reproduce the cylinder geometry and avoid adding an extra empty volume, which would reduce the compression ratio of the engine.

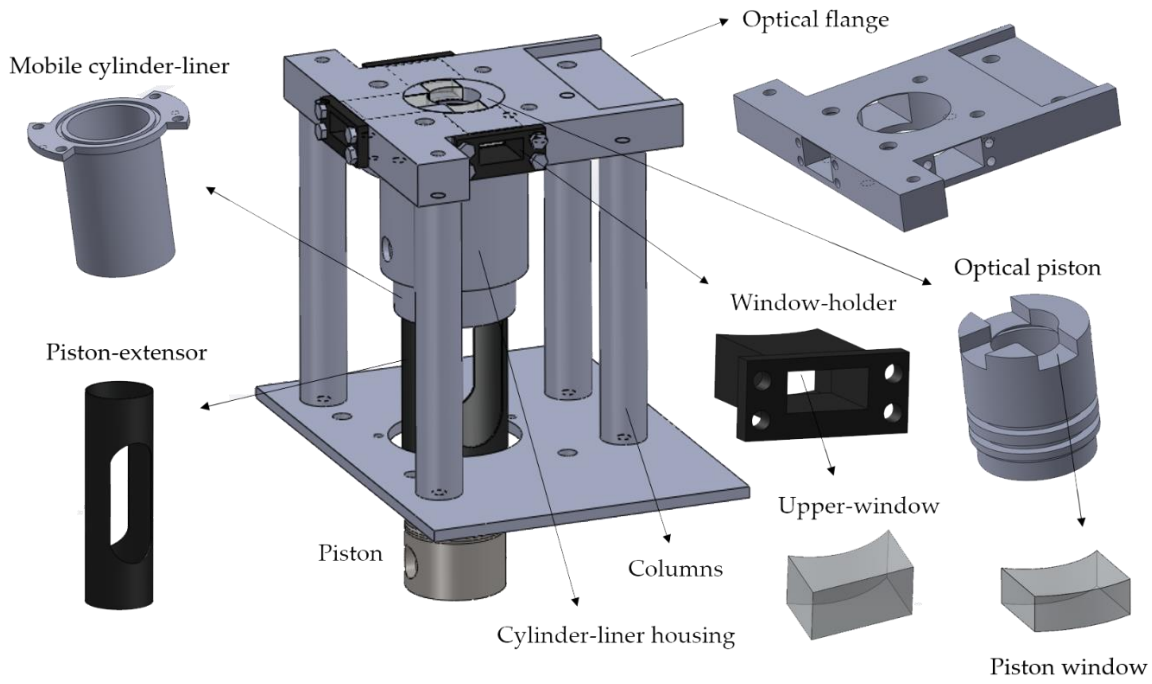

Figure 4. Assembly and individual view of the different components of the new design.

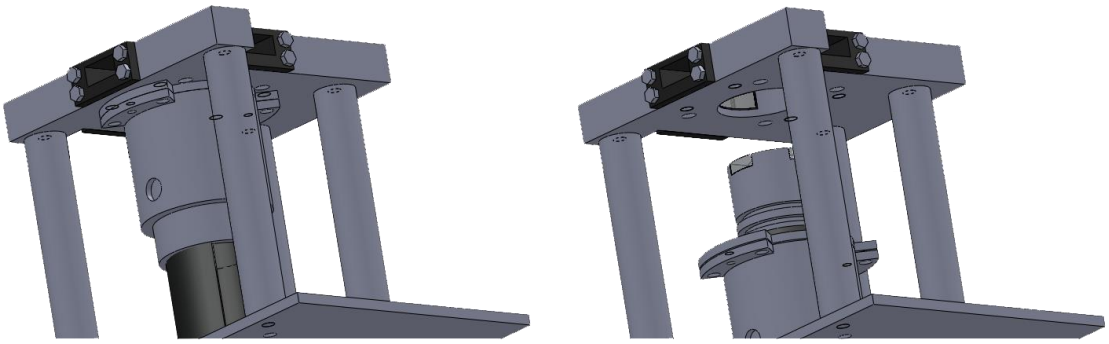

Figure 5. Illustration of the working (left) and cleaning position (right) with the new design.

To allow the optical access to the combustion chamber through the upper windows when the piston is located near the top dead center (TDC) position, three cuts where done in the piston head at positions aligned with each window (figure 6). To avoid losing compression ratio due to the additional empty volume introduced with the cuts in the piston head, three windows were glued in the gaps. The shape of the inner and the outer surfaces of the piston windows is rounded to follow the piston shape. The lateral surfaces of these windows, and therefore the cuts in the piston head, were designed with a conical shape. Although the windows were glued with a dedicated high-temperature resistant glue, the conical shape was conferred to prevent possible movements of the pistons due to the forces provoked by the high pressure and temperature gases in the inner surface.

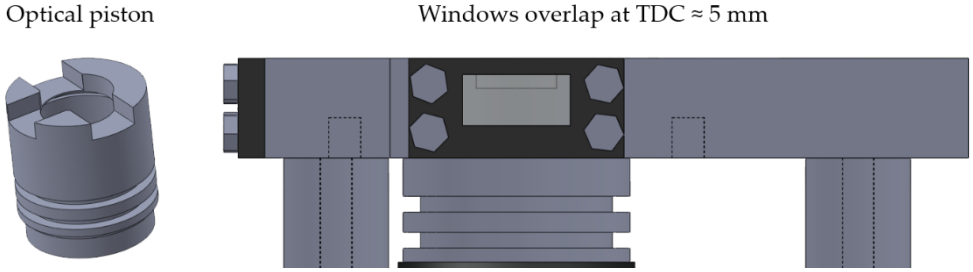

Figure 6. Optical piston (left) and illustration of the windows overlap at top dead center (right).

As explained before, the inner surface of the windows placed in the windows-holders and the windows used in the piston head, have a rounded shape to reproduce the geometry of the cylinder-liner and piston, respectively. This may have consequences if an optical technique using a laser sheet to illuminate the combustion chamber were used. In this sense, when passing through the windows, the laser sheet trajectory can be modify to be convergent or divergent due to the rounded shape of the windows, thus having a direct impact on the illuminated area of the combustion chamber. To evaluate this effect, a brief analysis was done using the OSLO (Optics Software for Layout and Optimization) software, whose results are shown in figure 7. As can be seen in figure 7a, which reproduces a situation in which the piston is not at TDC, the laser sheet becomes a little divergent at the outlet of the round side of the window. Figure 7b shows that, when both windows are aligned near TDC, the divergence is corrected at the outlet of the outer window, and it appears at the outlet of the piston window. In figures 7c and 7d, the laser sheet width at the inlet of the outer window has been set to maximize the illuminated area at TDC position. As can it be seen, the divergent effect is magnified at the outlet of the piston window, which is desirable to increase the illuminated area of the combustion chamber.

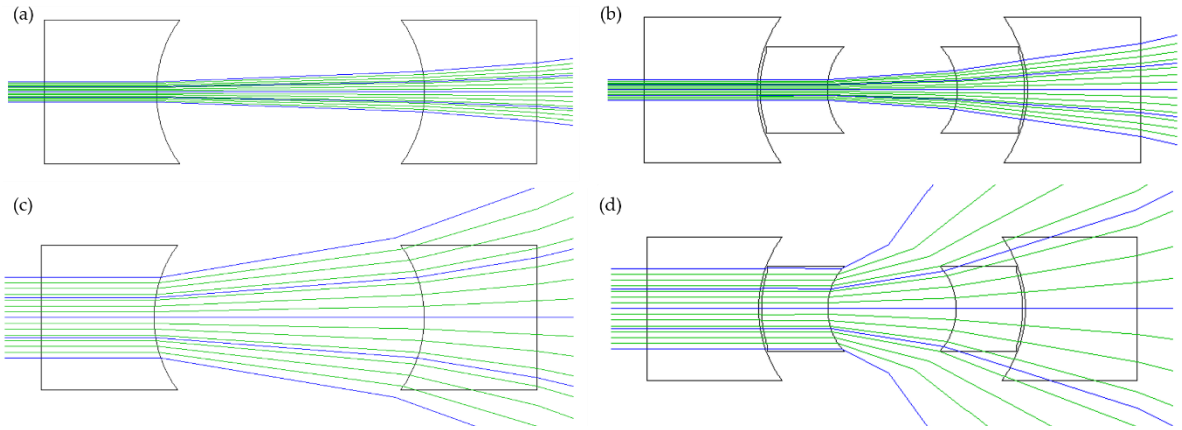

Figure 7. Effect of the windows shape on the laser sheet trajectory.

3.2. Engine characterization

A necessary task after the engine redesign is to evaluate if the characteristics of the new engine are representative of those of the real engines. For this purpose, this section shows the engine compression ratio and swirl ratio characterization with the new optical layout, explaining the methodology followed to characterize both parameters. Knowing this information will allow to realize, in a first approach, what is the range of in-cylinder conditions that could be analyzed in dedicated studies using the new engine platform.

3.2.1. Test cell characteristics

As figure 8 shows, to characterize the optical engine, it was installed in a fully instrumented test cell, with all the auxiliary facilities required for operation and control.

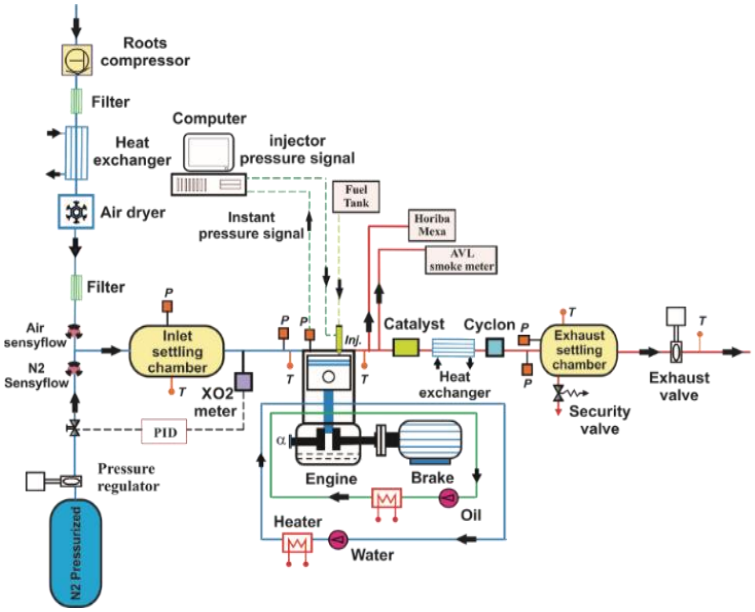

Figure 8. Test cell set-up to characterize the optical engine with the new design.

With this layout, the intake air is supplied by a roots compressor with an upper pressure limit of 3 bar. Then, the air flows through a filter to remove possible impurities. Independently on the ambient conditions, temperature and humidity of intake air are controlled using a heat exchanger and a dryer, respectively. Temperature in the inlet settling chamber is maintained constant by using a heater in the intake line.

During the engine characterization, the oxygen concentration variation is performed using a synthetic exhaust gas recirculation (EGR) system in order to achieve non-reactive conditions. EGR is substituted by nitrogen gas, which greatly simplifies the system ensuring a controllable gas composition without an excessive time to adjust the facility. The strategy is based on decreasing the oxygen (O_2) concentration at the inlet manifold by increasing the flow of nitrogen (N_2) and keeping constant the total intake mass flow rate (substitution EGR). For this purpose, a proportional-integral-derivative (PID) controller governed by the intake O_2 meter, is used to operate the N_2 valve. By contrast, when the engine is used for analyzing the combustion process, conventional EGR is used to not alter the engine-out emissions.

In the same way as in the intake line, a settling chamber is mounted in order to attenuate pressure pulses. Finally, an exhaust backpressure valve is used to maintain a fixed relative pressure to the intake pressure, in order to simulate more realistic conditions.

3.2.2. Effective compression ratio characterization

The compression ratio (CR) of an engine, defined in the equation 1, is a value that represents the ratio of the combustion chamber volume from its largest capacity (piston at BDC) to its smallest capacity (piston at TDC). In the equation 1, the term in brackets represents the volume at BDC, with *D* being the cylinder diameter and *S* the engine stroke. The term V_{min} is the minimum combustion chamber volume, which occurs when the piston is at TDC position, and accounts both the combustion chamber volume (V_{cc}) mechanized in the piston and the additional volume introduced by the cylinder-head gasket and other clearances.

$$CR = \frac{\left(\pi \cdot \frac{D^2}{4} \cdot S\right) + V_{min}}{V_{min}} \quad (1)$$

The actual CR of an engine typically differs from the one defined by the geometric parameters of the cylinder and combustion chamber (geometric CR) due to the precision of the machining process. One possible method to know the real CR is by filling the combustion chamber with a volume of fluid when the piston is at TDC position to know the term V_{min} of the equation 1. This procedure is not easy to carry out and introduces not negligible uncertainties on the measured value. An alternative procedure to characterize the CR is through

the in-cylinder pressure signal measurement under motored conditions [46]. This method is widely used and accepted by the engine research community, and is based on the polytropic adjustment of the pressure signal during the engine cycle, while the rate of heat release (RoHR) should be zero. The CR characterization of the new optical engine has been done following this procedure, for which, an in-house developed thermodynamic model called CALMEC [47][48] was used.

The CR characterization entails an iterative process in which several constants and coefficients must be adjusted, as illustrated in figure 9. In particular, the parameters and constants to be adjusted are the reference pressure (p_{ref}), TDC position (Δα), heat transfer constant (C_{W1}), mechanical deformations coefficient (k_{def}) and compression ratio (CR).

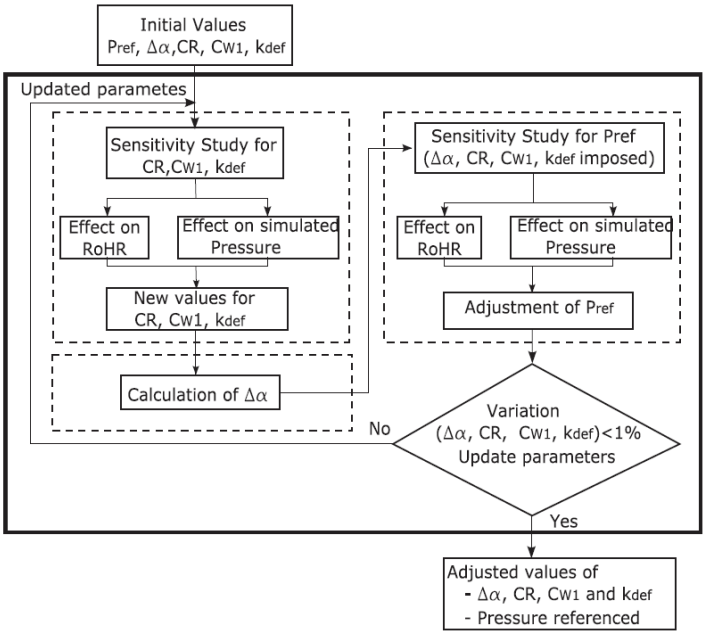

Figure 9. Scheme of the iterative process to characterize the engine [49].

As explained by Benajes et al. [49], p_{ref} and Δα can be determined by either experimental or thermodynamic methods, whose explanations are out of the scope of the current work. Nevertheless, it is interesting to remark that their correct characterization greatly affects the values of the rest of parameters. The heat transfer constant (C_{W1}) plays a key role inside the heat transfer model implemented in CALMEC. Heat transfer to the combustion chamber walls in motored tests (and fired tests) is essentially governed by convection. By this reason, the heat transfer model implemented in CALMEC to calculate the heat transfer coefficient is based on Woschni's expression. However, as described in a previous work [50], the values of the constants of the model have been modified, and the way in which the swirl effect is considered is also different to obtain more realistic predictions in direct injection engines. Thus, the expression used in CALMEC for the heat transfer coefficient is shown in equation 2:

$$h = CD^{-0.2}p^{0.8}T^{-053}\left[C_{W1}c_m + C_{W2}c_u + C_2\frac{v_d T_{IVC}}{v_{IVC}P_{IVC}}(p - p_0)\right]^{0.8} \qquad (2)$$

where C=0.12 and C_2=0.001, D is the cylinder diameter, p and T are the in-cylinder pressure and temperature, c_m is the mean piston speed, c_u is the instantaneous tangential velocity of the gas in the chamber due to the swirl motion (see [50] for the details of the calculation), C_{W1} is a constant fitted in the iterative process using data from motoring tests, C_{W2} value is C_{W1} divided by 1.7 [51], V_d and V_{IVC} are the displaced volume and the volume at the intake valve closing, respectively, and p_0 is the motoring pressure assuming a polytropic evolution.

At this point, the blow-by mass should be taken into account, because the amount of gas mass flowing to the outside of the cylinder will affect to the heat transfer, among others, and therefore to the CR adjustment. The blow-by model implemented in CALMEC is based on the evolution of the gas in an isentropic nozzle [52]. Thus, the instantaneous blow-by mass flow is estimated by means of the equation of an adiabatic nozzle, as shown in equation 3:

$$\mathrm{m_{bb}} = \mathrm{C}_{bb}\mathrm{A}_{ref}\mathrm{p}\sqrt{\frac{\mathrm{x}}{\mathrm{R}_c\mathrm{T}}} \quad (3) \text{ , where } \mathrm{x} = \frac{2\gamma}{(\gamma-1)}\left[\left(\frac{\mathrm{p}_{amb}}{\mathrm{p}}\right)^{\frac{2}{\gamma}} - \left(\frac{\mathrm{p}_{amb}}{\mathrm{p}}\right)^{\frac{\gamma+1}{\gamma}}\right] \quad (4)$$

In the equation 3, C_{bb} is the discharge coefficient of the nozzle, A_{ref} is the reference section proposed by Hohenberg [53] ($3.5\cdot10^{-6}D$), p_{amb} is the ambient pressure, and R_c and T are the compression ratio and temperature, respectively. The discharge coefficient (C_{bb}) should be adjusted iteratively using experimental measurements, for which, the authors used a dedicated part to measure the actual blow-by flow through the optical piston rings at different operating conditions (i.e. engine speed, intake pressure and intake temperature). This task is important to be done considering as much operating conditions as possible due to the particular characteristics of the piston rings used in the transparent engine.

The last parameter necessary to be adjusted for characterizing the effective compression ratio is the mechanical deformations coefficient (k_{def}), which is done by means of the mechanical deformations model. Through this model, the impact of the inertial and pressure forces on the effective compression ratio due to variations of the real in-cylinder volume, are accounted. To do this, the instantaneous volume is divided in four different terms, as shown in equation 5:

$$V(\alpha) = V_{cc} + V_d(\alpha) + \Delta V_p(\alpha) + \Delta V_i(\alpha) \quad (5)$$

- The combustion chamber volume is obtained by means of the equation 6, Where V_d is the displaced volume and r_c the geometric compression ratio of the engine.

$$V_{cc} = \frac{V_d}{r_c - 1} \quad (6)$$

- The instantaneous displaced volume $V_d(\alpha)$ depends on the connecting rod-crank mechanism, which includes the geometric offset if existing.
- The terms concerning the mechanical deformations due to pressure (ΔVp) and inertial (ΔV_i) forces are shown in the equations 7 and 8. In the equations, the term k_{def} is the deformations coefficient, which should be adjusted experimentally and typically has a value of 0.7 [54], which is taken as initial value for the iterative process. The term E_{steel} is the elastic modulus of the steel ($2.1\cdot10^{11}$ N/m^2), D_{bolt} is the piston bolt diameter, m_{alt} is the sum of masses with alternative movement, a is the instantaneous acceleration of the piston and L_0 is a characteristic length defined as equation 9.

$$\Delta V_p(\alpha) = k_{def} \cdot \frac{\pi D^2}{4} \cdot \frac{p}{E_{steel}} \cdot \left(\frac{D}{D_{bolt}}\right)^2 \cdot L_0 \quad (7)$$

$$\Delta V_i(\alpha) = k_{def} \cdot \frac{m_{alt} \cdot a}{E_{steel}} \cdot \left(\frac{D}{D_{bolt}}\right)^2 \cdot L_0 \quad (8)$$

With these considerations, it is hypothesized that the deformations of the engine will be proportional to those suffered by a steel bar of diameter equal to that of the piston bolt (D_{bolt}) and characteristic length equal to L_0 (equation 9). In the case of the inertial forces, the deformation is expected to occur in the piston, crank and connecting rod, while in the case of the pressure forces the deformation is supposed to occur in the piston, crank, connecting rod and engine block.

$$L_0 = h_{pis} + L_b + \frac{S}{2} \quad (9)$$

Considering mechanical deformations, the effective (or dynamic) compression ratio (CR_{eff}) can be defined as equation 10, where $\Delta V_{def}\ (TDC)$ is the sum of the pressure and inertial forces at TDC. By this way, the effective compression ratio is estimated considering the mechanical deformations occurring at TDC, where the volume is minimum and the deformations by pressure (greater than the inertial ones) are higher. With deformations at TDC around 2% or 3%, the dynamic compression ratio is between 0.3 and 0.5 less points than the geometric compression ratio (CR). Here it is interesting to note that, during firing operation, the loss in compression ratio due to mechanical deformations at TDC are partially compensated by the differences in thermal dilatation of the piston assembly with respect to the engine block.

$$CR_{eff} = \frac{V_d + V_{cc} + \Delta V_{def}(TDC)}{V_{cc} + \Delta V_{def}(TDC)} \quad (10)$$

The operating points measured under motored conditions to characterize the engine, are summarized in table 2. Each operating point was repeated 10 times and, to obtain an accurate characterization, 50 cycles were recorded each time. At these conditions, the coefficient of variation (COV) of the maximum in-cylinder pressure ranges from 0.1 to 0.16 % and the COV of the indicated mean effective pressure (IMEP) ranges from 0.3 to 0.66 %, respectively. This means that the engine is thermodynamically repeatable. The average pressure traces for the 500 cycles of each operating point are shown in figure 10. After applying the iterative process defined in figure 9, the effective compression ratio for the new design was found to be 14.2:1, 0.5 points less than the geometric one (14.7:1).

Table 2. Test matrix to characterize the engine under motored conditions.

Swirl valve [% open]	Intake pressure [bar]	n [rpm]	Exhaust pressure [bar]
100 0 50	1.5	900	1
100	1.1 1.9	900	1
100	1.5	600 1200	1

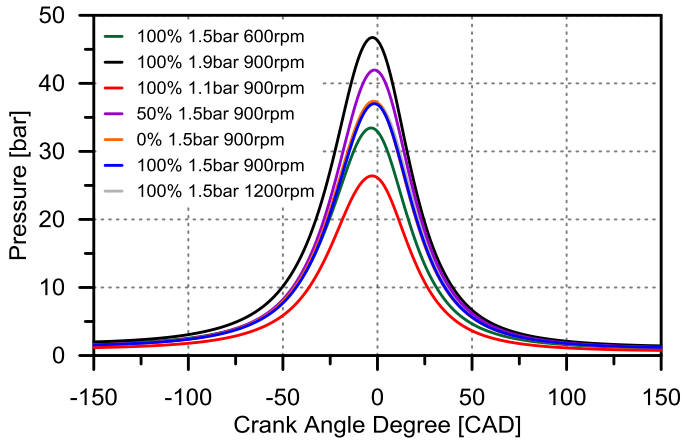

Figure 10. Motored in-cylinder pressure signal for the different cases summarized in table 2.

3.2.3. Swirl ratio characterization

The swirl ratio is a dimensionless parameter to quantify the rotational motion of the charge within the cylinder. This rotational motion is important to accelerate and enhance the air-fuel mixing process, which has a direct impact on the pollutant emissions formation and the rate of heat release.

A standard particle image velocimetry (PIV) system [55] was used for the measurement of instantaneous two-dimensional velocity fields, as shown in figure 11. The system main components are a double-head 15 Hz Nd:YAG laser with 135 mJ/pulse at a 532 nm wavelength, and a set of mirrors and lenses to drive the laser into the engine and change the laser output 5 mm circular beam into a laser sheet with around 1 mm thickness at the measurement section. The laser sheet passes through the optical accesses of the top work and piston head, and enables the illumination of particles seeded into the air intake flow.

After some preliminary tests with different kinds of seeding particles and generation methods, Aluminum Oxide (Al_2O_3) particles were selected. Several tests were made with different liquids generated with an atomizer using the Laskin nozzle principle (TSI 6-jet atomizer). It was found that the use of a silicon oil, test fluid and some other liquids was not possible because these fluids vaporized at the late compression stroke, thus avoiding the PIV measurements. To prevent this phenomenon, some tests were performed using titanium oxide solid particles generated with a fluidized bed and cyclone, but they presented high tendency to agglomerate, requiring frequent drying. This behavior made its use impractical in the engine test cell. A better behavior was found with Aluminum Oxide particles since, although degradation of the windows surface is known to occur faster, these particles do not tend to agglomerate so easily. Consequently, Al_2O_3 particles where dispersed with a pulsed fluidized bed device, followed by a specially designed cyclone which blocked out particles with estimated diameters higher than 5 µm, so that seeding particles are ensured to follow the engine flows hence measurements reliability is not limited by the size of the seeding particles.

The light scattered by the seeding particles was collected by a 4 megapixels CCD camera in two consecutive frames coincident with two laser shots by means of a synchronization box. Time elapsed between the two laser shots was set to 20 µs and was kept constant for all test points in the experimental test matrix. Based in these two frames, the particle position can be determined using cross-correlation algorithms. Hence, instantaneous two-dimensional velocity fields can be computed based on the displacement of particle groups within a given interrogation area of the image and the time step between frames. The magnification of the images taken was around 27 pixel/mm and the size of the interrogation area for calculation of the cross-correlations was set to 80x80 pixels. This leads to the measurement of velocity fields with vectors separated a distance of 40 pixels, i.e. 1.5 mm.

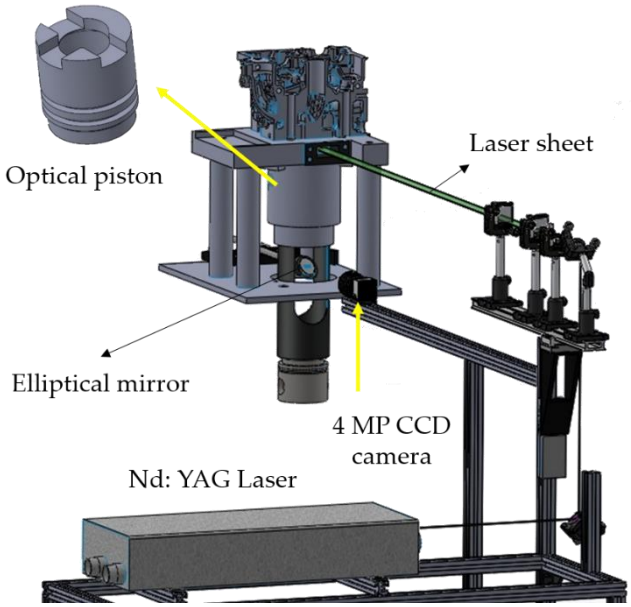

Figure 11. Optical set-up used to apply the particle image velocimetry (PIV) technique.

With this optical set-up, the swirl ratio can be characterized as described in figure 12. In particular, for a given crank-angle position, the swirl ratio (SR) is calculated by dividing the mean angular velocity of the air inside the cylinder and the crankshaft angular velocity (ω_{eng}) according to the equation 11.

$$SR = \frac{\sum_{i=1}^{N} \omega_i}{\omega_{eng} N} \quad (11)$$

In-cylinder air load angular velocity is calculated from the ensemble average velocity field (figure 12), as the tangential component of velocity divided by the distance relative to cylinder axis following the equation 12.

$$\omega_i = \frac{\vec{V_i} \cdot \vec{e_\perp}}{|\vec{r_i}|} \quad (12)$$

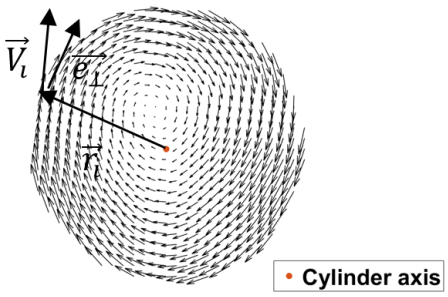

Figure 12. Velocity vectors after processing the image taken trough particle image velocimetry (PIV) technique.

Following the procedure previously explained, the swirl ratio of the engine was characterized in motored conditions (without combustion) and 1200 rpm for different laser timings referred to the piston position. As shown in figure 13, the swirl ratio varies between 1 and 1.7 depending on the timing considered, showing a general increasing trend as the piston moves towards TDC. This occurs because, as the piston approaches the TDC during the compression stroke, more gas is confined in a smaller cavity. Thus, the moment of inertia of the in-cylinder gas decreases and the angular velocity (and thus the swirl ratio) increases, as shown in figure 14.

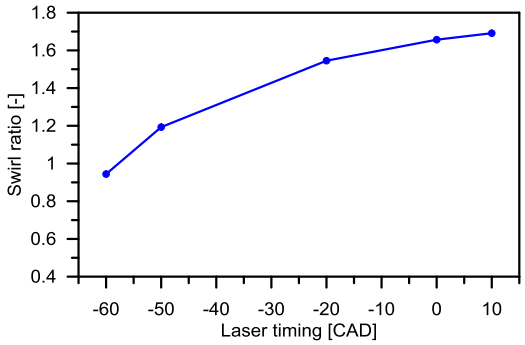

Figure 13. Calculated swirl ratio from the PIV images for different laser timings.

Figure 14 shows the velocity fields, standard deviations and vortex centers at the timings of the extreme cases of swirl ratio, -60 and +10 CAD ATDC. Comparing both figures, it can be seen that, as piston moves towards TDC, the average velocity field increases. The increase of the velocity field is more evident for distances farther than 10 mm from the geometric center, where increments up to 1.5 m/s are found in some areas. Some differences are also found in the center of the image. In particular, a near quite flow field it is seen in the case of -60 CAD ATDC, while values between 0.5 and 1 m/s are found for +10 CAD ATDC. Finally, it is also seen that the standard deviation of the velocity field decreases for crank timings near TDC and the vortex center is nearer the geometric center of the combustion chamber in this case.

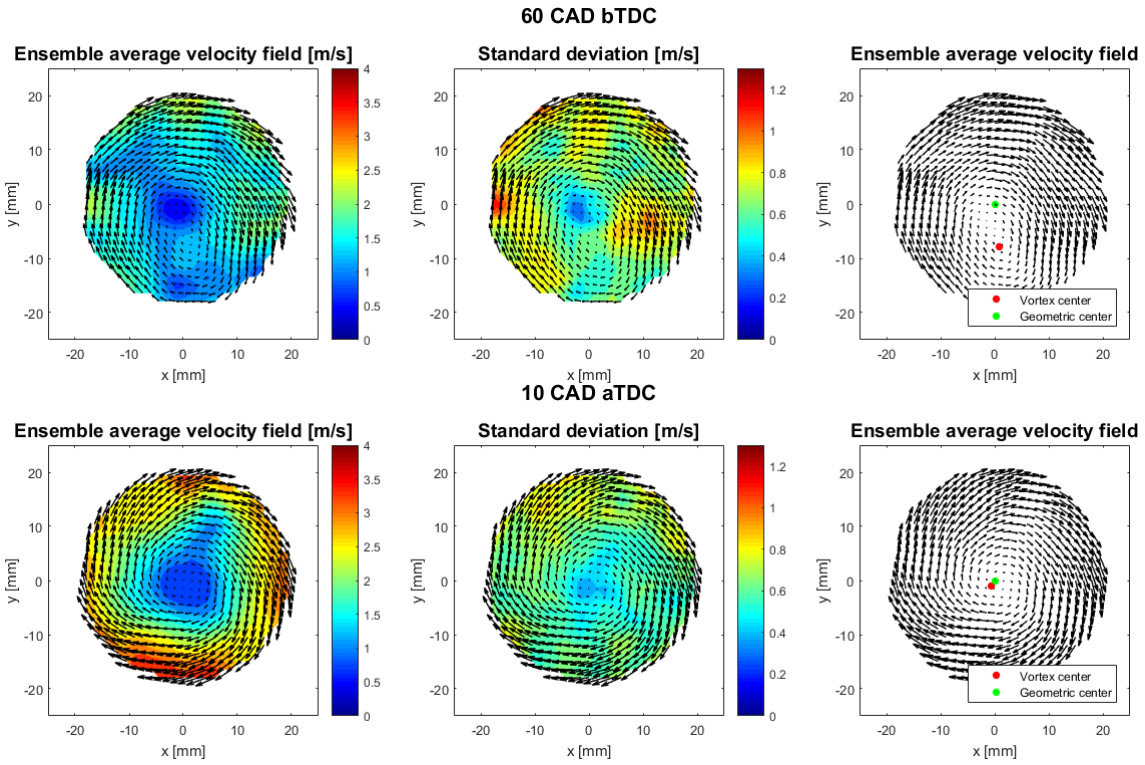

Figure 14. PIV results from the images taken through the piston window for laser timings set at -60 and +10 CAD ATDC, which corresponds to the extreme cases of swirl ratio.

4. Conclusions

The present work has described the redesign and characterization processes of an optical engine to maximize the optical accessibility and its operating efficiency. The main drawbacks found during the operation with the original design, were highlighted first. In this sense, the major source of operating inefficiency is the excessive time consumed to clean the optical parts. The piston window cleaning takes around 40 minutes, while the substitution of the piston rings takes around 4-5 hours due to the need of disassembling the cylinder-head.

To minimize these shortcomings, a modular design was proposed instead of using a single piece top work. New design main components are: four columns, a new optical top work in which three windows are placed using windows-holders, three piston windows accommodated in the piston head, and a metal piece acting as base joining the new assembly with the engine block. A key part of the new design are the window-holders, which allow fitting the upper-windows in the optical flange. This assembly method allows a fast transition between optical and metal engine, and also a very fast cleaning procedure. In this sense, the time consumed to clean all the optical parts and replace the piston rings is around 10 and 8 minutes, respectively.

The new optical engine was mounted in a fully instrumented test cell for its characterization. The effective compression ratio of the new optical engine was found to be 14.2:1, similar to the geometric one (14.7:1). The swirl ratio was characterized at 1200 rpm under motored conditions by means of the particle image velocimetry (PIV) technique using Aluminum Oxide seeding particles. The results of this study revealed swirl ratios varying from 1 to 1.7 depending on the timing considered. The lowest swirl ratio was found at the earliest timing tested (-60 CAD ATDC) and the highest one at +10 CAD ATDC.

Acknowledgments

This work has been partially funded by the Spanish Government under the project HiReCo TRA2014-58870-R. The equipment used has been partially funded by FEDER project ICTS-2012-06, framed in the operational program of unique scientific and technical infrastructure of the Ministry of Science and Innovation of Spain. The author J. Monsalve-Serrano acknowledges the financial support from the Universitat Politècnica de València under the grant “Ayudas Para la Contratación de Doctores para el Acceso al Sistema Español de

Ciencia, Tecnología e Innovación". The authors wish to thank Daniel Lérida for his technical work during the redesign process.

References

1. Dargay J.; Gately D. Income's effect on car and vehicle ownership, worldwide: 1960-2015. Transportation Research Part A: Policy and Practice 1999, 33 (2), 101-138.
2. European Automobile Manufacturers' Association. The Automobile Industry Pocket Guide 2014-2015. Technical report 2015.
3. Energy, Transport and Environment Indicators. Technical report 2014.
4. Environmental Protection Agency. Nitrogen Oxides (NOx), Why and How They Are Controlled. Technical report 1999.
5. Environmental European Agency. Emissions of primary PM2.5 and PM10 particulate matter. Technical report 2013.
6. Regulation (EC) 595/2009 of the European Parliament and of the Council of 18 June 2009 on type-approval of motor vehicles and engines with respect to emissions from heavy duty vehicles (Euro VI) and on access to vehicle repair and maintenance information and amending Regulation (EC) 715/2007 and Directive 2007/46/EC and repealing Directives 80/1269/EEC, 2005/55/EC and 2005/78/EC. Official Journal of the European Union 2009, 52 (275), 1-14.
7. Pastor J.V.; García-Oliver J.M.; García A.; Micó C.; Möller S. Application of optical diagnostics to the quantification of soot in n-alkane flames under diesel conditions. Comb and Flame 2016, 164, 212-223.
8. Desantes J.M.; Pastor J.V.; García-Oliver J.M.; Briceño F.J. An experimental analysis on the evolution of the transient tip penetration in reacting Diesel sprays. Comb and Flame 2014, 161 (8), 2137-2150.
9. Desantes J.M.; Arregle J.M.; Lopez J.J. Scaling laws for free turbulent gas jets and diesel-like sprays. Atomization Sprays 2006, 16, 443-473.
10. Desantes J.M.; Torregrosa A.J.; Broatch A. Experiments on Flow Noise Generation in Simple Exhaust Geometries. Acustica 2001, 87 (1), 46-55.
11. Benajes J, García A, Monsalve-Serrano J, Boronat V. Achieving clean and efficient engine operation up to full load by combining optimized RCCI and dual-fuel diesel-gasoline combustion strategies. Energy Conversion and Management, Volume 136, 15 March 2017, Pages 142-151.
12. Payri R.; Gimeno J.; Bardi M.; Plazas A. Study liquid length penetration results obtained with a direct acting piezo electric injector. Appl Energy 2013, 106, 152-162.
13. Garcia A.; Monsalve-Serrano J.; Heuser B.; Jakob M.; Kremer F.; Pischinger S. Influence of fuel properties on fundamental spray characteristics and soot emissions using different tailor-made fuels from biomass. Energy Conv and Manag 2016, 108, 243-254.
14. An H.; Chung J.; Lee S.; Song S. The effects of hydrogen addition on the auto-ignition delay of homogeneous primary reference fuel/air mixtures in a rapid compression machine. Int Journal of Hydrogen Energy 2015, 40 (40), 13994-14005.
15. Payri F.; Desantes J.M.; Pastor J.V. LDV measurements of the flow inside the combustion chamber of a 4-valve D.I. diesel engine with axisymmetric piston-bowls. Exp in Fluids 1996, 22(2), 118-128.
16. Benajes J.; Molina S.; García A.; Monsalve-Serrano J.; Durrett R. Conceptual model description of the double injection strategy applied to the gasoline partially premixed compression ignition combustion concept with spark assistance. Appl Energy 2014, 129, 1-9.
17. Desantes J.M.; Lopez J.J.; García J.M. Evaporative diesel spray modeling. Atomization Sprays 2007, 17, 193-231.
18. Battistoni M.; Mariani F.; Risi F.; Poggiani C. Combustion CFD Modeling of a Spark Ignited Optical Access Engine Fueled with Gasoline and Ethanol. Energy Procedia 2015, 82, 424-431.
19. Benajes J.; García A.; Pastor J.M.; Monsalve-Serrano J. Effects of piston bowl geometry on Reactivity Controlled Compression Ignition heat transfer and combustion losses at different engine loads. Energy 2016, 98, 64-77.
20. Benajes J.; García A.; Monsalve-Serrano J.; Balloul I.; Pradel G. An assessment of the dual-mode RCCI/CDC capabilities in a EURO VI medium-duty diesel engine fueled with an intermediate ethanol-gasoline blend and biodiesel. Energy Conv and Manag 2016, 123, 381-391.

21. Benajes J.; Martín J.; García A.; Villalta D.; Warey A. In-cylinder soot radiation heat transfer in direct-injection diesel engines. Energy Conv and Manag 2015, 106, 414-427.
22. Luján J.M.; Climent H.; Dolz V.; Moratal A.; Borges-Alejo J.; Soukeur Z. Potential of exhaust heat recovery for intake charge heating in a diesel engine transient operation at cold conditions. Appl Thermal Eng 2016, 105, 501-508.
23. Bohla T.; Tiana G.; Zengb W.; Heb X.; Roskilly A. Optical Investigation on Diesel Engine Fuelled by Vegetable Oils. Inter Conf on Appl Energy, ICAE2014. Energy Procedia 2014, 61, 670–674.
24. Bizon K.; Continillo G.; Lombardi S.; Sementa P.; Vaglieco B. Independent component analysis of cycle resolved combustion images from a spark ignition optical engine. Comb and Flame 2016, 163, 258–269.
25. Mancaruso E.; Sequino L.; Vaglieco B. Analysis of the pilot injection running Common Rail strategies in a research diesel engine by means of infrared diagnostics and 1d model. Fuel 2016, 178, 188–201.
26. Zeng W.; Sjöberg M.; Reuss D.; Hu Z. High-speed PIV, spray, combustion luminosity, and infrared fuel-vapor imaging for probing tumble-flow-induced asymmetry of gasoline distribution in a spray-guided stratified-charge DISI engine. Proc of the Comb Inst 2016, 1–8. 10.1016/j.proci.2016.08.047.
27. Catapano F.; Sementa P.; Vaglieco B. Air-fuel mixing and combustion behavior of gasoline-ethanol blends in a GDI wall-guided turbocharged multi-cylinder optical engine. Renew Energy 2016, 96, 319-332.
28. Merola S.; Tornatore C.; Irimescu A.; Marchitto L.; Valentino G. Optical diagnostics of early flame development in a DISI (direct injection spark ignition) engine fueled with n-butanol and gasoline. Energy 2016, 108, 50-62.
29. Marseglia G.; Costa M.; Catapano F.; Sementa P.; Vaglieco B. Study about the link between injection strategy and knock onset in an optically accessible multi-cylinder GDI engine. Energy Conv and Manag 2017, 134, 1–19.
30. Irimescu A.; Merola S.; Tornatore C.; Valentino G. Effect of coolant temperature on air-fuel mixture formation and combustion in an optical direct injection spark ignition engine fueled with gasoline and butanol. Journal of the Energy Inst 2016, 1-14. http://dx.doi.org/10.1016/j.joei.2016.03.004.
31. Irimescu A.; Merola S.; Valentino G. Application of an entrainment turbulent combustion model with validation based on the distribution of chemical species in an optical spark ignition engine. App Energy 2016, 162, 908–923.
32. Pastor J.V.; García-Oliver JM.; García A.; Pinotti M. Laser induced plasma methodology for ignition control in direct injection sprays. Energy Conv and Manag 2016, 120, 144-156.
33. Regan C.; Chun, K.; and Schock H. Engine Flow Visualization using a Copper Vapor Laser. Proc SPIE: New developments and Applications in Gas Lasers 1987, 737, 17-27.
34. Le Coz J.-F.; Henriot S.; and Pinchon P. An Experimental and Computational Analysis of the Flow Field in a Four-Valve Spark Ignition Engine-Focus on Cycle-Resolved Turbulence. SAE tech paper 1990, 900056.
35. Catapano F.; Sementa P.; Vaglieco Bianca. Optical characterization of bio-ethanol injection and combustion in a small DISI engine for two wheels vehicles. Fuel 2013, 106, 651–666.
36. Bowditch F. Cylinder and Piston Assembly. US Patent 1958, App. 2,919,688, 2,919,688.
37. Pastor JV.; J.M. García-Oliver JM.; A. García A.; Micó C.; Durrett R. A spectroscopy study of gasoline partially premixed compression ignition spark assisted combustion. App Energy 2013, 104, 568–575.
38. Di Iorio S.; Sementa P.; Vaglieco B. Analysis of combustion of methane and hydrogen–methane blends in small DI SI (direct injection spark ignition) engine using advanced diagnostics. Energy 2016, 108, 99–107.
39. Sementa P.; Vaglieco Bianca.; Catapano F. Thermodynamic and optical characterizations of a high performance GDI engine operating in homogeneous and stratified charge mixture conditions fueled with gasoline and bio-ethanol. Fuel 2012, 96, 204–219.
40. Richman R.; Reynolds W. The Development of a Transparent Cylinder Engine for Piston Engine Fluid Mechanics Research. SAE tech paper 1984, 840379.
41. Bates S. A Transparent Engine for Flow and Combustion Visualization Studies. SAE tech paper 1988, 880520.
42. Zhang Y.; Zhang R.; Rao L.; Kim D.; Kook S. The influence of a large methyl ester on in-flame soot particle structures in a small-bore diesel engine. Fuel 2017, 194, 423–435.
43. Reuss D. Cyclic Variability of Large-Scale Turbulent Structures in Directed and Undirected IC Engine Flows. SAE tech paper 2000, 2000-01-0246.

44. López J.J.; García-Oliver J.M.; García A.; Domenech V. Gasoline effects on spray characteristics, mixing and auto-ignition processes in a CI engine under Partially Premixed Combustion conditions. Appl Thermal Eng 2014, 70 (1), 996-1006.
45. Benajes J.; García A.; Domenech V.; Durrett R. An investigation of partially premixed compression ignition combustion using gasoline and spark assistance. Appl Thermal Eng 2013, 52 (2), 468-477.
46. Klein M.; Eriksson L.; Åslund J. Compression ratio estimation based on cylinder pressure data. Control Eng Practice 2006, 14 (3), 197–211.
47. Payri F.; Olmeda P.; Martín J.; García A. A complete 0D thermodynamic predictive model for direct injection diesel engines. Appl Energy 2011, 88 (12), 4632-4641.
48. Payri F.; Olmeda P.; Martin J.; Carreño R. A New Tool to Perform Global Energy Balances in DI Diesel Engines. SAE Int. J. Eng. 2014, 7(1), 2014-01-0665.
49. Benajes J.; Olmeda P.; Martín J.; Carreño R. A new methodology for uncertainties characterization in combustion diagnosis and thermodynamic modelling. Appl Therm Eng 2014, 71, 389-399.
50. Payri F.; Margot X.; Gil A.; Martín J. Computational study of the heat transfer to the walls of a DI diesel engine. SAE tech paper 2005, 2005-01-0210.
51. Martín J. Diagnóstico de la combustión en motores de Diesel de inyeccióon directa. Reverté, Barcelona, España, 2012, ISBN 978-84-291-4717-9.
52. Payri F.; Galindo J.; Martín J.; and Arnau F. A Simple Model for Predicting the Trapped Mass in a DI Diesel Engine. SAE tech paper 2007, 2007-01-0494.
53. Hohenberg G. Definition und Eigenschaften des thermodynamischen Verlustwinkels von Kolbenmaschinen. Automobil-Industrie 1976, 4, 15–21.
54. Armas O. Diagnóstico experimental del proceso de combustión en motores Diesel de inyección directa. Doctoral Thesis 1998, Universitat Politècnica de València.
55. Berna C.; Juliá J.E.; Escrivá A.; Muñoz-Cobo J.L.; Pastor J.V.; Micó C. Experimental investigation of the entrained droplet velocities in a submerged jet injected into a stagnant water pool. Exp Thermal and Fluid Sci 2017, 82, 32-41.